Thermal Handprint Analysis for Forensic Identification using Heat-Earth Mover's Distance

Kun Woo Cho[1], Feng Lin[1], Chen Song[1], Xiaowei Xu[1], Fuxing Gu[2], and Wenyao Xu[1]

[1]Department of Computer Science and Engineering, SUNY at Buffalo
[2]Shanghai Key Lab of Modern Optical System, University of Shanghai for Science and Technology

Abstract

Recently, handprint-based recognition system has been widely applied for security and surveillance purposes. The success of this technology has also demonstrated that handprint is a good approach to perform forensic identification. However, existing identification systems are nearly based on the handprints that could be easily prevented. In contrast to earlier works, we exploit the thermal handprint and introduce a novel distance metric for thermal handprint dissimilarity measure, called Heat-Earth Mover's Distance (HEMD). The HEMD is designed to classify heat-based handprints that can be obtained even when the subject wears a glove. HEMD can effectively recognize the subjects by computing the distance between point distributions of target and training handprints. Through a comprehensive study, our identification system demonstrates the performance even with the handprints obtained by the subject wearing a glove. With 20 subjects, our proposed system achieves an accuracy of 94.13% for regular handprints and 92.00% for handprints produced with latex gloves.

1. Introduction

In recent years, biometrics has emerged as a novel method of forensic identification that makes use of physical traits intrinsic to each person [17, 12]. The most widely used biometric features include face, fingerprint, voice, gait and iris. Face and fingerprint biometrics are commonly employed, while they are easily hidden using hat and gloves. Gait and voice biometrics are also vulnerable when the subject intends to change the features for spoofing. Iris is a robust biometric feature, however, its information requires an expensive device and specific condition to acquire. In contrast, handprint contains very rich and distinctive biometric information. Therefore, it can be extracted from low-resolution images with a relatively high accuracy. Combin-

ing all of the geometric features, including length and width of fingers, palm geometry, and principal lines, it is possible to create a highly accurate identification system [14].

Many algorithms have been developed for handprint-based identification in the last several years. For instance, Ying *et al.* presented the hand texture based personal identification methods, which utilizes whole hand skin image for recognition [17]. Similarly, Yan *et al.* proposed a handprint-based verification system by integrating a hand geometry feature and a finger-print feature. This algorithm, composed of a coarse matching, wavelet zero crossing, and fine level identification stage, has the accuracy of 97.00% [16]. The success of such algorithms demonstrates the reliability and stability of using handprints for personal identification. However, the above mentioned algorithms require the images that are clearly visible to human eyes and to conventional cameras. When introduced in forensic casework, it is difficult to obtain a clear image of handprint if a subject avoids to leave his imprint.

Recently, thermal imaging has been investigated on its physical traits, such as material properties [2], thermal reflection [11], and has become favorable for various applications, such as surveillance systems [13], security systems [9], and human-computer interactive systems [7, 8]. In these systems, a thermal camera not only detects the object but also traces heat signatures left behind by body parts touching a surface. Although this technology is used in many areas, to the best of our knowledge, so far there is no related work using thermal imaging for biometrics-based forensic personal identification. We exploit the infrared thermography in extracting handprint for personal identification for following reasons: i) it expands target extent by capturing any object with a temperature above zero; ii) thermal handprint can be obtained regardless of illumination or direct contact [3], which is more robust than other visible light-based imaging; iii) it is cost-effective compared to the high-resolution camera used in extracting detailed features

of fingerprint.

In this paper, we propose a forensic identification system incorporating heat-based handprints and a novel distance metric, heat-earth mover's distance (HEMD) that is specifically designed for thermal handprint recognition. K nearest neighbors (kNN) classification is further used to classify the subjects. To validate the effectiveness of our method, we comprehensively evaluate the system performance based on the several accuracy metrics, receiver operating characteristic curve as well as an equal error rate. Our identification system achieves an accuracy of 94.13% for standard handprints and 92.00% for subjects wearing latex gloves, as well as 95.69% and 98.50% for area under the curve (AUC). Their degree of and closeness in accuracy and AUC prove the concept of biometric identification based on thermal handprint is feasible and promising even with the subjects wearing a glove.

This paper is structured as follows: Section 2 reviews the thermographic background. Section 3 describes the development of the thermal handprint identification system, which is subdivided into pre-processing, HEMD algorithm, and classification with k-Nearest Neighbor. Then, Section 4 provides a description and discussion on the performance evaluation. Finally, Section 5 draws the conclusion.

2. Infrared Emission

Invisible to human eyes, infrared radiation is emitted by any objects that has a temperature above the absolute zero. The amount of infrared radiation is affected by the temperature and emissivity, as described by Stefan-Boltzmanns law: [3]:

$$W = \sigma \cdot \varepsilon \cdot T^4 \qquad (1)$$

where W is the total amount of energy emitted per square meter (W/m^2), σ is the Stefan-Boltzmann constant ($5.6705 \times 10^{-8} W m^2/K^4$), T is the temperature (K) of the object surface, and ε is the emissivity, a measure of the efficiency in which a surface emits thermal energy.

2.1. Emissivity

Emissivity of an object varies from 0 to 1 according to its material, wavelength, and the surface texture [3]. Theoretical object with a perfect emissivity ($\varepsilon = 1$) is referred as a black body, an object capable of absorbing all the incident radiation [4]. According to Plank's law, the radiation emission from a black body is described as follow [5]:

$$\frac{\partial R(\lambda, T)}{\partial \lambda} = \frac{2\pi h c^2 \lambda^{-5}}{exp(\frac{hc}{\lambda k T}) - 1}, \qquad (2)$$

where the first term represent the spectral radiation from a black body, h is the plank constant ($6.6256 \times 10^{-34} Js$), k is the Boltzmanns constant ($1.38054 \times 10^{-23} JK^{-1}$), c is the speed of light ($2.998 \times 10^8 ms^{-1}$), and λ is the wavelength.
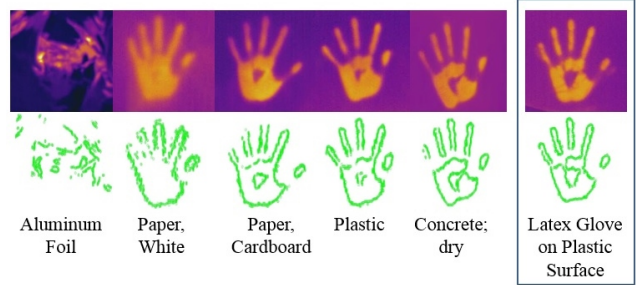

Figure 1: Effect of emissivity on the clarity of raw thermal images and contour points of handprint.

Table 1: Emissivity coefficient of surface materials [1]

Common Surface Material	Emissivity Coefficient
Aluminum foil	0.05
Paper, white	0.68
Cardboard, white	0.81
Rubber, natural soft (latex)	0.86
Plastic	0.94
Concrete, dry white	0.95

However, perfect black bodies do not exist in nature and the above law does not apply to our handprints without certain correction. According to Kirchhoffs Law, non-black bodies absorb a fraction A, reflect a fraction R and transmit a fraction T of the incident radiation [5]. Since the amount of absorbance equals the amount of emission at thermal equilibrium, the relationship is shown as follow:

$$\varepsilon(\lambda) + \tau(\lambda) + \rho(\lambda) = 1. \qquad (3)$$

where τ is the transmittance, and ρ is the reflectance. When third equation is applied to Plank's law, radiation emission of real existent objects can be expressed as follow [5]:

$$\frac{\partial R(\lambda, T)}{\partial \lambda} = \varepsilon(\lambda) \frac{\partial R_{blackbody}(\lambda, T)}{\partial \lambda}, \qquad (4)$$

$\varepsilon(\lambda)$ is an emissivity coefficient for the energy being emitted by an object relative to that emitted by a black body. According to the equation, increase in the emissivity coefficient of non-black body object increases the amount of spectral radiation emitted by the object. Since infrared camera forms a brightness with respect to the amount of radiation emitted, clarity of our handprint is dependent on the emissivity coefficient of the surface as it is shown in Fig. 1 and Table 1. For surface with a extremely low emissivity coefficient like aluminum foil, thermal handprint cannot be obtained.
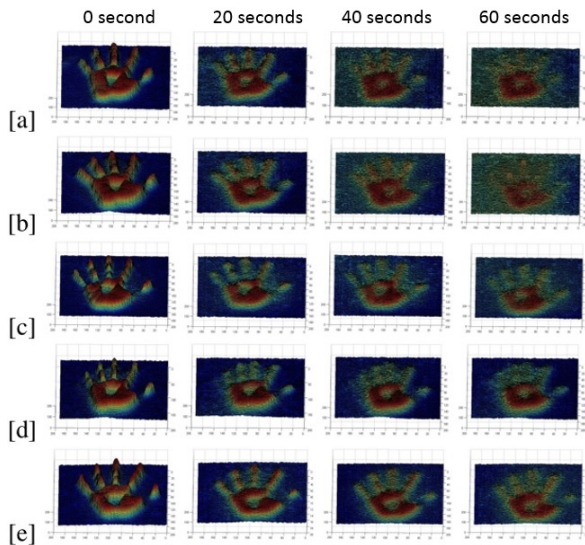
Figure 2: Effect of surface material on the rate of cooling for 1 minute: (a) paper (b) cardboard (c) latex on the plastic surface (d) plastic (e) concrete

2.2. Duration

Although thermal handprints can be obtained from the wide range of objects, they tend to dissipate in a rapid manner depending on the material of contacted surface, temperature of surrounding, and initial temperature of body parts touching a surface.

Fig. 2 provides a three dimensional illustration of the visibility on thermal handprints as they cool down to room temperature. Height and color of the hand figures are equivalent to the temperature of handprint. When the entire plate reaches a uniform intermediate room temperature, thermal handprint is eventually invisible on the infrared camera. In the illustrations, images are captured for every 20 seconds with different surface materials, including paper, cardboard, plastic, and concrete. All trials are done in the similar setting; after pressing for 10 seconds, heat trails are left alone at room temperature for 1 minute.

Materials with a relatively low emissivity coefficient like paper and cardboard tend to absorb and diffuse heat in the larger surface area but cool down relatively quickly. In contrast, materials like plastic and concrete absorb heat in the smaller surface area but the shape of handprint on theses materials is clearly visible throughout 60 seconds. Also, the initial handprint image on the materials with higher emissivity coefficient shows much clearer characteristic of palm and index fingers compared to that of lower emissivity.

Fig. 3 is a graphical representation of Fig. 2 with a longer period of time. Images are captured for every 30 seconds from 0 second to 120 seconds. Y-value of the graph is representing the average color scale of the handprint, and the horizontal dashed line at 55.1 index implies the average
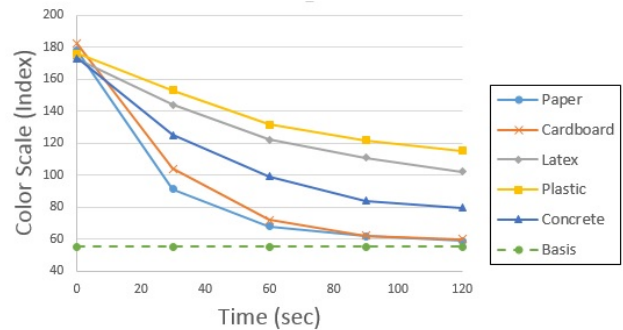

Figure 3: Rate of cooling for different surface materials: paper, cardboard, latex on the plastic surface, plastic, and concrete. The horizontal dashed line in green implies the temperature of the color scale of non-contacted surface

color scale of non-contacted area (basis). Therefore, it is a minimum possible color scale value of the handprint. When y-value of a certain handprint reaches the basis, investigator is unable to capture the image of handprint. When exponential function is applied, y-value of the handprint and the basis intersect at 104 seconds, 112 seconds, 151.4 seconds, 276.78 seconds, and 283.5 seconds respectively for paper, cardboard, concrete, latex, and plastic. These values at the point of intersection imply the duration. In fact, duration of the handprint produced with latex glove is only 6.72 seconds apart from that of plastic surface. Since both cases are taken on the same surface material (plastic), their slight difference in duration indicates that wearing latex glove merely affects the dissipation of heat and duration of the thermal handprint.

3. Algorithm

The handprint-based personal identification with HEMD is shown in Fig. 4. It roughly illustrates the five main components: thermal camera, pre-processing, HEMD, kNN classification, and monitoring. Details of pre-processing, HEMD, and kNN classification are discussed in this section.

3.1. Pre-processing

For each image, pre-processing is required to improve the result of later processing. In pre-processing, following steps are adopted: cropping, gray-scaling, and noise filtering. Using adobe photo-shop cs6, we apply an automatic mass/batch crop to the images, so every images can be 192×192 pixel dimension. For second step, we convert these RGB images into gray scale. Then we filter the images with 2-D median filter to remove the noise without reducing the sharpness of the image. For median filter, each output pixel is set to an median of the pixel values in the neighborhood of the corresponding input pixel. Possible effect of noise is prevented in this process. Feature detection
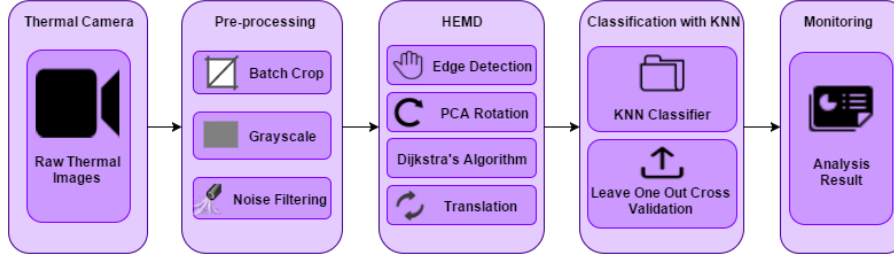
Figure 4: Handprint recognition framework.

| Thermal Input | Grayscale | Noise filtering | Sobel edge detection | PCA rotation | Contour detection |

Figure 5: Feature extraction in different steps of the algorithm. The features are extracted from subject 1.

and rotation are involved with HEMD, which are discussed in the following section.

3.2. Heat-Earth Mover's Distance

As shown in Fig. 5, HEMD uses a Sobel filter for edge detection algorithm. This edge detection algorithm finds the boundaries of objects within images by computing an approximation of the gradient of the image intensity function with two 3×3 kernels - one for horizontal changes, and one for vertical changes.

To increase the accuracy, the images must be closely aligned. Thus, HEMD adopts principal component analysis (PCA) to estimate the angle of the major axis of variation and to rotate the image according to the variation. The rotation angel is equal to the angle between the first eigenvectors of the PCA results and the edge of the image [15].

Then, we formulate the task of hand recognition as matching between two sets. Earth mover's distance (EMD) is suitable for such a problem as it has been proved to be a robust distance metrics for image retrieval by Rubner et al [10]. It is defined as a minimal cost that must be paid to transform one distribution into another. In HEMD, there is a target handprint X with m clusters of points, where x_i is the cluster representative and w_{x_i} is the weight of the cluster. Target X is required to supply training handprint Y with n clusters of points, where y_j is the capacity representative and w_{y_j} is the weight of the cluster. For Y, each points acts as a predefined consumer of the point from X. For each target-training pair, the cost of transporting a single point is given. The transportation problem is then to find a least-expensive flow of points from the target to the training that satisfies the training's demand [10].

The target and training are represented as follow: target $X = \{(x_1, w_{x_1}) \cdots (x_m, w_{x_m})\}$, $1 \leq i \leq m$, and training

$Y = \{(y_1, w_{y_1}) \cdots (y_n, w_{y_n})\}$, $1 \leq j \leq n$; and $D = [d_{ij}]$ the ground distance matrix where d_{ij} is the ground distance between clusters x_i and y_j. We want to find a flow $F = [f_{ij}]$, that transports the points from the target to the training with the least cost [10]:

$$HEMD(X,Y,F) = min(\sum_{i=1}^{m}\sum_{j=1}^{n} f_{ij}d_{ij}) \quad (5)$$

with subject to

$$f_{ij} \geq 0; 1 \leq i \leq m, 1 \leq j \leq n \quad (6)$$

$$\sum_{i=1}^{m} w_{x_i} = \sum_{j=1}^{n} w_{y_j} \quad (7)$$

$$\sum_{j=1}^{n} f_{ij} \leq w_{x_i}; 1 \leq i \leq m \quad (8)$$

$$\sum_{i=1}^{m} f_{ij} \leq w_{y_j}; 1 \leq j \leq n \quad (9)$$

$$\sum_{i=1}^{m}\sum_{j=1}^{n} f_{ij} = min(\sum_{i=1}^{m} w_{x_i}, \sum_{j=1}^{n} w_{y_j}) \quad (10)$$

First constraint allows moving points from X to Y but not from X to Y. Second constraint states that the overall weight of points in X equals the overall weight of points in Y and therefore, weight normalization is not required. Third constraint limits the amount of points in target that can be sent by the clusters in X to their weights. Then, fourth constraint limits the clusters in Y from receiving points more than their capacity. The last constraint forcefully moves the maximum amount of points, which is also referred as a total flow [10]. Once the transportation is done, HEMD is defined as the resulting work normalized by the total flow:

$$HEMD(X,Y) = \frac{\sum_{i=1}^{m}\sum_{j=1}^{n} f_{ij}d_{ij}}{\sum_{i=1}^{m}\sum_{j=1}^{n} f_{ij}} \quad (11)$$

Fig. 6 illustrates two transportation problems: one with the same subject and one with the different subject. There are m number of green points, x_i, and n number of red
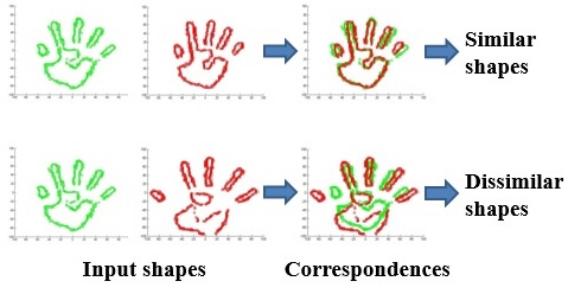
Figure 6: Heat-earth mover's distance

points, y_j. When colored points are in correspondence, $cost$ between target and training points is defined by Euclidean distance. For every Euclidean distances, Dijkstra's algorithm is applied to find the shortest paths between nodes. It fixes a single node and finds shortest path from the source to all other nodes, producing a shortest path tree.

3.3. Classification with k nearest neighbors

The k-nearest neighbors (kNN) classifier assigns a new object to the most common class among-st the most similar k objects in the data set [6]. Labeled training data $T = \{(a_i, b_i)\}$ while $a_i \in \mathbb{R}^p$ and label $b_i \in \{1, \cdots, j\}$. New unlabeled test data is $a \in \mathbb{R}^p$. Our task is to predict the label of a, which can be represented as b. In this experiment, $a_i \in \{HEMD_{0,0} \cdots HEMD_{n,n}\}$; $b_i \in \{Subject_1 \cdots Subject_{20}\}$; $a = HEMD_{target}$. Our distance function is HEMD and k equals 5.

4. Performance Evaluation

To evaluate the feasibility and effectiveness of HEMD, we implement various performance metrics for biometric system. They include accuracy (ACC), balanced accuracy (BAC), and f-measure accuracy, receiver operating characteristics (ROC), and equal error rate (EER).

4.1. Hardware unit

Thermal handprints are captured by a hand held thermal camera (model IRS 75). Its optic resolution is 160×120 pixels with an image flame rate of 60Hz. IRS 75 has a temperature range of -20° C to $+350^\circ$ C, but the instrument generates an automatic calculation of the temperature difference. Its noise equivalent temperature difference (NETD) has less than or equal to 0.6° C thermal sensitivity at $+30^\circ$ C. Focal plane array detector (FPA) used for this model captures the wavelength range of 7.5 μm to 13 μm. This camera calibrates automatically based on the input optical transmittance and has a laser pointer to help positioning the target.

During the experiment, thermal camera is held by a 350 mm tripod. Lens is perpendicularly located to a blow-
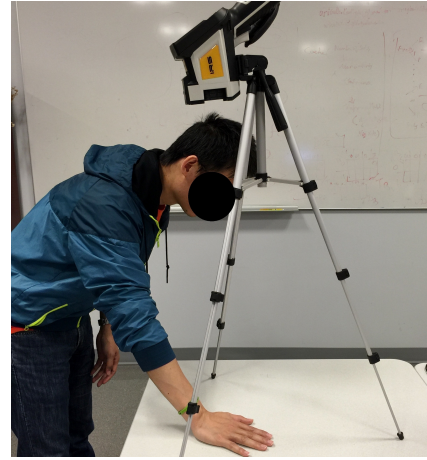

Figure 7: Infrared imaging system IRS 75 in use

molded plastic surface. Their vertical distance is approximately 29.7 inches for all shootings.

4.2. Evaluation description

There are 20 subjects in the experiment, where 17 subjects are male and 3 subjects are female. Their ages are in the range of 18 to 35. During the experiment, two types of sample, Standard-Handprint (SH) and Glove-Handprint (GH), are investigated. For SH sample, 40 images are collected for each subject and for GH sample, 20 images are collected for each subject. Thus, total amount of SH is 800 and total amount of GH is 400. Both methods follow the same camera set-up as it is depicted in Fig. 7.

Leave-one-out-cross-validation (LOOCV) is used to test the proposed approach. For standard handprint, one SH image is selected as a target data and the rest SH images are regarded as a training data. This process is repeated for each 800 SH images. For handprint made with latex glove, one GH image is selected as a target data and the rest GH images are regarded as a training data. This process is repeated for each 400 GH images.

4.3. Identification scenario

To evaluate the system in the forensic scenario, the multi-suspect with a single criminal scene is established. There are two scenarios simulated where the criminal left his or her thermal handprint without the latex glove and with the latex glove. Each of 20 subjects is selected once as a criminal and the rest of the subjects are the people whom HEMD must reject. Two-classification module is set up where the criminal's data is the positive class and the rest data is the negative class. Based on leave-one-out-cross-validation, each data set of every class becomes the target data for one time and every data except for the selected target data becomes the training data.

4.4. Experimental results

To measure how well a binary classification test identifies the subject, three accuracy metrics, ACC, BAC and F1, are adopted. First accuracy (ACC) metric is defined as:

$$Accuracy(\%) = \frac{TP + TN}{TP + FP + TN + FN} \times 100\% \quad (12)$$

where TP is the true positive, TN is the true negative, FP is the false positive and FN is the false negative. The average accuracy for SH and GH is 94.13% and 92.00%.

For second accuracy measure, balanced accuracy metric (BAC) is adopted. BAC is known for avoiding inflated performance estimates on imbalanced dataset. By definition, it is the arithmetic mean of sensitivity and specificity:

$$BAC(\%) = \frac{sensitivity + specificity}{2} \quad (13)$$

$$= \frac{0.5 \times TP}{TP + FN} + \frac{0.5 \times TN}{TN + FP} \quad (14)$$

As shown in Table 2, we achieved BAC value of 94.49% for SH and and 92.50% for GH with standard deviation of 8.59% and 9.09% respectively.

For third accuracy metric, we use a F-measure accuracy measure (F1), which the recall and precision are evenly weighted. It is also known as a harmonic mean of precision and recall. Following metric is defined as:

$$F1(\%) = 2 \times \frac{Precision \times Recall}{Precision + Recall} \quad (15)$$

According to the confusion matrix in Table 3, the average precision and recall of classifications for SH are 94.85% and 94.13% respectively, and its f-measure accuracy is 94.49%. According to the confusion matrix for GH sample images, shown in Table 4, the average precision and recall are 93.00% and 92.00% respectively, and the f-measure accuracy is 92.50%. The accuracy difference between two methods is only 1.99%, which indicates that our HEMD can obtain a highly accurate result even when the subject wears a glove. This can be interpreted by the fact that heat easily penetrates the glove. Also, although latex has relatively lower emissivity than plastic, the emissivity is much less influential than the temperature as shown in Stefan-Boltzmann's law.

Table 2: Performance comparison for SH and GH

Sample Type	ACC (%)	BAC (%)	F1 (%)
SH	94.13	94.49± 8.59	94.49
GH	92.00	92.50± 9.09	92.50
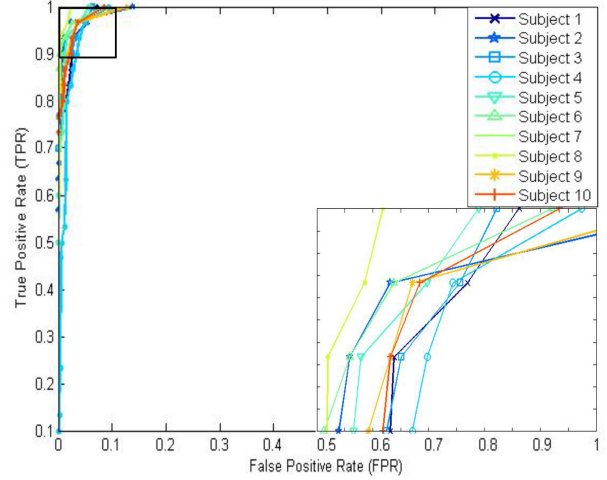
Figure 8: The ROC curve of 10 out of 20 subjects for SH and its close-up image.
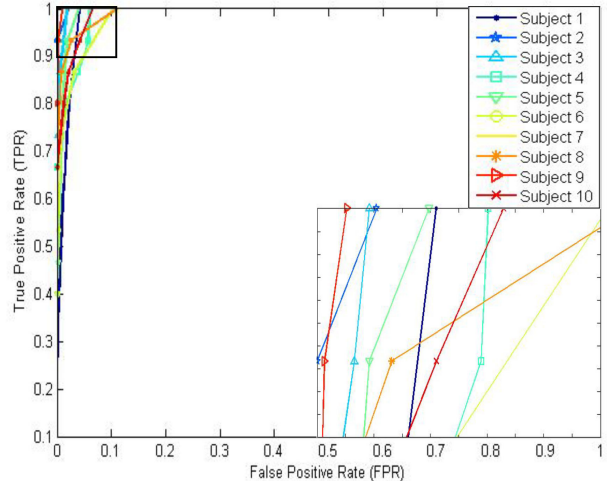
Figure 9: The ROC curve of 10 out of 20 subjects for GH and its close-up image.

4.4.1 Receiver operating characteristic (ROC)

To inspect the classifier more closely, ROC curves are investigated for two sample types. ROC curve is an effective method to visually assess how the classifier performs in the region of high sensitivity and high specificity. By definition, it is a plot of TPR against FPR for different thresholds of the classifier output. The closer the curve follows the left and top portion of the ROC space, the more accurate the test is. In ROC, two error rates, FNR and FPR, are traded off against each other. If the classification is carried out in a very strict setup, FNR and FPR are extremely low that every subjects, including a criminal, will be unidentified.

Table 3: Standard handprint confusion matrix with subject A-T

subject	A	B	C	D	E	F	G	H	I	J	K	L	M	N	O	P	Q	R	S	T	Recall (%)
A	40	0	0	0	0	0	0	0	0	0	0	0	0	0	0	0	0	0	0	0	100
B	0	38	0	1	0	0	0	0	0	0	0	0	0	0	0	0	0	0	1	0	95.0
C	0	0	40	0	0	0	0	0	0	0	0	0	0	0	0	0	0	0	0	0	100
D	0	0	0	34	0	0	0	0	0	0	0	0	1	0	0	0	0	5	0	0	85.0
E	0	0	0	0	40	0	0	0	0	0	0	0	0	0	0	0	0	0	0	0	100
F	0	0	0	0	0	40	0	0	0	0	0	0	0	0	0	0	0	0	0	0	100
G	0	0	0	2	0	0	37	0	0	0	0	0	0	0	0	0	1	0	0	0	92.5
H	2	0	0	0	0	0	0	37	0	0	0	0	0	0	0	0	0	0	1	0	92.5
I	0	0	0	1	0	0	0	0	39	0	0	0	0	0	0	0	0	0	0	0	97.5
J	0	0	0	0	0	0	0	0	0	40	0	0	0	0	0	0	0	0	0	0	100
K	0	0	0	0	0	0	0	0	0	0	40	0	0	0	0	0	0	0	0	0	100
L	0	0	0	1	0	0	0	0	0	0	0	39	0	0	0	0	0	0	0	0	97.5
M	0	0	0	5	0	0	0	0	0	0	0	0	35	0	0	0	0	0	0	0	87.5
N	0	0	0	0	0	0	0	0	0	0	0	0	0	40	0	0	0	0	0	0	100
O	0	0	0	1	0	0	0	0	0	0	0	0	0	0	39	0	0	0	0	0	97.5
P	0	0	0	0	0	0	0	0	0	0	0	0	0	0	0	40	0	0	0	0	100
Q	1	0	0	0	0	0	0	0	0	0	0	0	0	0	0	0	39	0	0	0	97.5
R	0	0	0	6	0	0	0	0	0	8	0	0	0	0	0	0	0	26	0	0	65.0
S	2	0	1	0	0	0	0	2	0	0	0	0	0	0	0	0	1	0	34	0	85.0
T	0	0	0	4	0	0	0	0	0	0	0	0	0	0	0	0	0	0	0	36	90.0
Precision (%)	88.9	100	97.6	61.8	100	100	100	94.9	100	83.3	100	100	97.2	100	100	100	95.1	83.9	94.4	100	94.13

Table 4: Latex glove handprint confusion matrix with subject A-T

subject	A	B	C	D	E	F	G	H	I	J	K	L	M	N	O	P	Q	R	S	T	Recall (%)
A	16	0	0	0	0	0	0	0	0	4	0	0	0	0	0	0	0	0	0	0	80.0
B	0	20	0	0	0	0	0	0	0	0	0	0	0	0	0	0	0	0	0	0	100
C	0	0	15	0	0	0	0	0	1	0	0	0	0	0	0	0	0	0	0	4	75.0
D	0	0	0	16	0	0	0	0	0	0	0	0	0	0	0	4	0	0	0	0	80.0
E	1	0	0	0	19	0	0	0	0	0	0	0	0	0	0	0	0	0	0	0	95.0
F	0	0	0	0	2	18	0	0	0	0	0	0	0	0	0	0	0	0	0	0	90.0
G	0	0	0	0	0	0	20	0	0	0	0	0	0	0	0	0	0	0	0	0	100
H	0	0	0	0	0	0	0	18	0	0	0	0	0	0	2	0	0	0	0	0	90.0
I	0	0	0	0	0	0	0	0	20	0	0	0	0	0	0	0	0	0	0	0	100
J	0	0	0	0	0	0	0	0	0	20	0	0	0	0	0	0	0	0	0	0	100
K	1	0	0	0	0	0	0	0	0	0	19	0	0	0	0	0	0	0	0	0	95.0
L	0	0	0	0	2	0	0	0	0	0	0	18	0	0	0	0	0	0	0	0	90.0
M	0	0	0	0	0	0	0	0	0	0	0	0	20	0	0	0	0	0	0	0	100
N	0	0	0	0	0	0	0	0	0	0	1	0	0	17	0	1	0	1	0	0	85.0
O	0	0	0	0	0	0	0	0	0	0	0	0	0	0	20	0	0	0	0	0	100
P	0	0	0	0	0	0	0	0	0	0	0	0	0	0	0	20	0	0	0	0	100
Q	0	0	0	0	0	0	0	0	0	0	0	0	0	0	0	0	20	0	0	0	100
R	2	0	0	0	0	0	0	0	0	0	1	0	0	0	0	0	0	17	0	0	85.0
S	0	0	0	0	0	0	0	0	0	0	0	0	0	0	0	0	0	0	20	0	100
T	5	0	0	0	0	0	0	0	0	0	0	0	0	0	0	0	0	0	0	15	75.0
Precision (%)	64.0	100	100	100	82.6	100	100	100	95.2	83.3	90.5	100	100	100	90.9	80.0	100	94.4	100	79.0	92.00

Along with the ROC curve, the area under the curve (AUC) is provided to show how well a parameter can distinguish a targeted subject.

Fig. 8 and Fig. 9 display the ROC curves for SH and GH. In each figures, only the curves for 10 subjects out of 20 are depicted for the reader's convenience. The average AUC of 20 subjects for SH and GH are 95.69% and 98.50% respectively with standard deviation of 6.91% and 2.40%. The performance of SH and GH in Fig. 8 and Fig. 9 shows a similarity except that GH is more linearly upward while SH is curved to right. This phenomenon is partially affected by the difference in sample size as SH has 40 samples for each subject and GH has 20 samples for each subject.
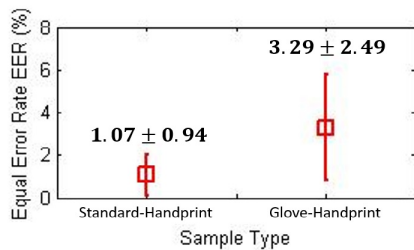
4.4.2 Equal error rate (EER)

Figure 10: Equal Error Rate (EER) for SH and GH. The error-bars are indicating the standard deviation of EER among 20 subjects

The Equal Error Rate (EER) is a performance metric for biometric systems. It is a rate when the operating threshold for the accept and reject decision is adjusted such that the acceptance error (FPR) and rejection error (FNR) become equal. The lower the equal error rate value, the higher the accuracy of the biometric system. As shown in Figure 10, SH and GH have EER of 1.07% and 3.29% with respective standard deviations of 0.94% and 2.49%. Both sample types have small percentage of EER and narrow standard deviation, which indicates the high accuracy of HEMD. However, the relatively low EER of SH suggests that using handprint without the glove is more stable and distinguishable than using handprints made with the glove.

5. Conclusion

In this paper, we present a novel HEMD method for thermal handprint recognition. Unlike previously published works, our system has accurately classified the data regardless of prevention. Comprehensive experiments are conducted and achieved the accuracy of 94.13%. For handprint with latex glove, the average accuracy is 92.00%. The performance results indicate that HEMD is secure and feasible biometric system.

Acknowledgement

References

[1] Infrared thermometer emissivity tables. Technical report, Scigiene Corporation, 2006.

[2] Y. Abdelrahman, A. Sahami Shirazi, N. Henze, and A. Schmidt. Investigation of material properties for thermal imaging-based interaction. In *Proceedings of the 33rd Annual ACM Conference on Human Factors in Computing Systems*, CHI '15, pages 15–18, New York, NY, USA, 2015. ACM.

[3] G. J. Edelman, R. J. Hoveling, M. Roos, T. G. Leeuwen, and M. C. Aalders. Infrared imaging of the crime scene: possibilities and pitfalls. *Journal of forensic sciences*, 58(5):1156–1162, 2013.

[4] G. Gaussorgues and S. Chomet. *Infrared thermography*, volume 5. Springer Science & Business Media, 2012.

[5] G. Ginesu, D. D. Giusto, V. Märgner, and P. Meinlschmidt. Detection of foreign bodies in food by thermal image processing. *Industrial Electronics, IEEE Transactions on*, 51(2):480–490, 2004.

[6] D. J. Hand, H. Mannila, and P. Smyth. *Principles of data mining*. Adaptive Computation and Machine Learning series. MIT press, 2001.

[7] S. G. Kong, J. Heo, F. Boughorbel, Y. Zheng, B. R. Abidi, A. Koschan, M. Yi, and M. A. Abidi. Multiscale fusion of visible and thermal ir images for illumination-invariant face recognition. *International Journal of Computer Vision*, 71(2):215–233, 2007.

[8] W.-H. Liao and C.-M. Yang. Video-based activity and movement pattern analysis in overnight sleep studies. In *Pattern Recognition, 2008. ICPR 2008. 19th International Conference on*, pages 1–4. IEEE, 2008.

[9] K. Mowery, S. Meiklejohn, and S. Savage. Heat of the moment: Characterizing the efficacy of thermal camera-based attacks. In *Proceedings of the 5th USENIX Conference on Offensive Technologies*, WOOT'11, pages 6–6, Berkeley, CA, USA, 2011. USENIX Association.

[10] Y. Rubner, C. Tomasi, and L. J. Guibas. The earth mover's distance as a metric for image retrieval. *International journal of computer vision*, 40(2):99–121, 2000.

[11] A. Sahami Shirazi, Y. Abdelrahman, N. Henze, S. Schneegass, M. Khalilbeigi, and A. Schmidt. Exploiting thermal reflection for interactive systems. In *Proceedings of the 32nd annual ACM conference on Human factors in computing systems*, pages 3483–3492. ACM, 2014.

[12] C. Song, A. Wang, K. Ren, and W. Xu. Eyeveri: A secure and usable approach for mobile user authentication. In *IEEE International Conference on Computer Communication (Infocom'16)*, 2016.

[13] W. K. Wong, H. L. Lim, C. K. Loo, and W. S. Lim. Home alone faint detection surveillance system using thermal camera. In *Computer Research and Development, 2010 Second International Conference on*, pages 747–751. IEEE, 2010.

[14] X. Wu, D. Zhang, and K. Wang. Fusion of phase and orientation information for palmprint authentication. *Pattern analysis and applications*, 9(2-3):103–111, 2006.

[15] X. Xu, F. Lin, A. Wang, C. Song, Y. Hu, and W. Xu. On-bed sleep posture recognition based on body-earth movers distance. In *IEEE Biomedical Circuits and Systems Conference (BioCAS 15)*, 2015.

[16] H. Yan and D. Long. A novel bimodal identification approach based on hand-print. In *Image and Signal Processing, 2008. CISP'08. Congress on*, volume 4, pages 506–510. IEEE, 2008.

[17] H. Ying, T. Tieniu, S. Zhenan, and H. Yufei. Identity verification by using handprint. In *Advances in Biometrics*, pages 328–337. Springer-Verlag Berlin Heidelberg, 2007.